

Toward the Development of Molecular Wires: Ruthenium(II) Terpyridine Complexes Containing Polyferrocenyl as a Spacer

Teng-Yuan Dong,* Kellen Chen, Mei-Ching Lin, and Liangshiu Lee

Department of Chemistry, Center for Nanoscience and Nanotechnology, National Sun Yat-Sen University, Kaohsiung, Taiwan, Republic of China

Received April 19, 2005

The preparations of multinuclear supramolecules assembled from 1,1'-bis(terpyridyl)ferrocene, 1,1'-bis(terpyridyl)biferrocene, and 1,1'-bis(terpyridyl)triferrocene (tpy-(fc)_n-tpy, *n* = 1–3) redox-active moieties with Ru²⁺ metal centers are described. The electrochemical measurements of the Ru²⁺ complexes of tpy-(fc)_n-tpy (**1a** (*n* = 1); **1b** (*n* = 2); **1c** (*n* = 3)) are dominated by the Ru²⁺/Ru³⁺ redox couple (*E*_{1/2} from 1.35 to 1.38 V), Fe²⁺/Fe³⁺ redox couples (*E*_{1/2} from ~0.4 to ~1.0 V), and tpy/tpy⁻/tpy²⁻ redox couples (*E*_{1/2} from -1.3 to -1.5 V). The appreciable variations detected in the Fe²⁺/Fe³⁺ oxidation potentials indicate that there is an interaction between the spacer and the Ru²⁺ metal centers. Coordination of Ru²⁺ metal centers to tpy-(fc)_n-tpy results in a red-shifted and more intense ¹[(d(π)_{Fe})⁶] → ¹[(d(π)_{Fe})⁵-(π*_{tpy}^{Ru})¹] transition in the visible region. The observed red-shifted absorption from 526 nm in the monomeric [Ru(fctpy)₂]²⁺ complex to ~560 nm in **1b** and **1c** reveals that there is a qualitative electronic coupling within the ferrocenyl array. The Fe–Fe interactions result in a red characteristic of the ¹[(d(π)_{Fe})⁶] → ¹[(d(π)_{Fe})⁵(π*_{tpy}^{Ru})¹] MMLCT transition.

Introduction

The development of molecular wires where photoactive and electroactive terminals are linked by a large-size molecular spacer may open new paths in the field of storage and utilization of light energy. An important issue concerns how best to interlock the spacer into an ordered array that permits controlled transfer of stored information along the molecular axis. In principle, this issue can be resolved by careful manipulation of the energetics of the photoactive and electroactive terminals and of the connecting spacer. In general, the design principle combines the most unsaturated form of organic linear spacer with the most stable redox-active terminals. The application of redox-active ferrocenyl groups as built-in electrochemical sensors to evaluate the degree of electronic communication through the spacer has been described.¹ Our design principle for a molecular wire has to fulfill following criteria: (i) an organometallic redox-active spacer to enhance the capability of transfer information along the molecular axis and (ii) modular synthetic approach to control length. To address these items, we chose bis(2,2':6',2''-terpyridyl)polyferrocene as the spacer connected to electroactive Ru²⁺ metal terminals.

Recently, the design of new interesting bis-2,2':6',2''-terpyridine ligands (tpy-tpy) by connecting two terpyridine moieties via a rigid organic spacer attached to their 4'-positions has received a surge in interest^{2–4} that

has found applications in energy conversion systems such as dye-sensitized solar cells⁵ and electroluminescent devices.⁶ The tpy-tpy ligands that have been prepared and used further to make dinuclear transition metal complexes are illustrated in Chart 1.^{7–20}

(2) Balzani, V.; Scandola, F. *Supramolecular Photochemistry*; Ellis Horwood: Chichester, 1991.

(3) (a) Sauvage, J.-P.; Collin, J.-P.; Chambron, J.-C.; Guillerez, S.; Coudret, C.; Balzani, V.; Barigolletti, F.; Cloa, L. De; Flamigni, L. *Chem. Rev.* **1994**, *94*, 993. (b) Harriman, A.; Ziessel, R. *Coord. Chem. Rev.* **1998**, *171*, 331. (c) Barigolletti, F.; Flamigni, L. *Chem. Soc. Rev.* **2000**, *29*, 1.

(4) Collin, J.-P.; Gaviña, P.; Heitz, V.; Sauvage, J.-P. *Eur. J. Inorg. Chem.* **1998**, *1*.

(5) (a) Hagfeldt, A.; Grätzel, M. *Acc. Chem. Res.* **2000**, *33*, 269. (b) Bignozzi, C. A.; Argazzi, R.; Kleverlaan, C. J. *Chem. Soc. Rev.* **2000**, *29*, 87. (c) Wang, P.; Zakeeruddin, S. M.; Moser, J. E.; Nazeeruddin, M. K.; Sekiguchi, T.; Grätzel, M. *Nat. Mater.* **2003**, *2*, 402. (d) Islam, A.; Sugihara, H.; Arakawa, H. *J. Photochem. Photobiol., A* **2003**, *158*, 131.

(6) (a) Slinker, J.; Bernards, D.; Houston, P. L.; Abruna, H. D.; Bernhard, S.; Malliaras, G. G. *Chem. Commun.* **2003**, 2392. (b) Kalyuzhny, G.; Buda, M.; McNeill, J.; Barbara, P.; Bard, A. J. *J. Am. Chem. Soc.* **2003**, *125*, 6272. (c) Welter, S.; Brunner, K.; Hofstraal, J. W.; De Cola, L. *Nature* **2003**, *421*, 54.

(7) Indelli, M. T.; Scandola, F.; Collin, J.-P.; Sauvage, J.-P.; Sour, A. *Inorg. Chem.* **1996**, *35*, 303.

(8) Patoux, C.; Launay, J.-P.; Beley, M.; Chodorowski-Kimmes, S.; Collin, J.-P.; James, S.; Sauvage, J.-P. *J. Am. Chem. Soc.* **1998**, *120*, 3717.

(9) Beley, M.; Chodorowski-Kimmes, S.; Collin, J.-P.; Lainé, P.; Launay, J.-P.; Sauvage, J.-P. *Angew. Chem., Int. Ed. Engl.* **1994**, *33*, 1775.

(10) Schütte, M.; Kurth, D. G.; Linford, M. R.; Cölfen, H.; Möhwald, H. *Angew. Chem., Int. Ed.* **1998**, *37*, 2891.

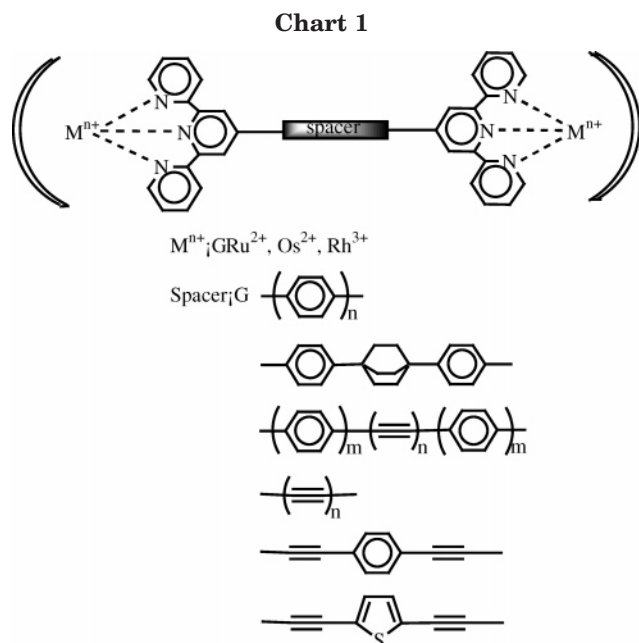
(11) Hammarström, L.; Barigolletti, F.; Flamigni, L.; Armaroli, N.; Sour, A.; Collin, J.-P.; Sauvage, J.-P. *J. Am. Chem. Soc.* **1996**, *118*, 11972.

(12) Grosshenny, V.; Harriman, A.; Gisselbrecht, J.-P.; Ziessel, R. *J. Am. Chem. Soc.* **1996**, *118*, 10315.

(13) Benniston, A. C.; Grosshenny, V.; Harriman, A.; Ziessel, R. *Angew. Chem., Int. Ed. Engl.* **1994**, *33*, 1884.

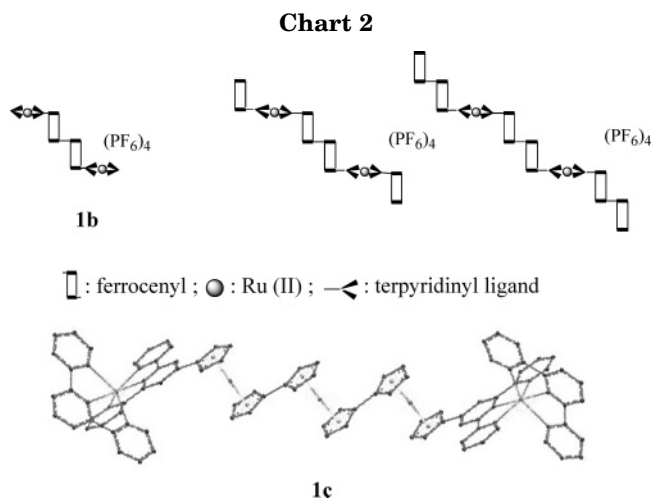
(14) Grosshenny, V.; Harriman, A.; Ziessel, R. *Angew. Chem., Int. Ed. Engl.* **1995**, *34*, 2705.

(1) (a) Geiger, W. E. *J. Organomet. Chem. Libr.* **1990**, *22*, 142. (b) Skibar, W.; Kopacka, H.; Wurst, K.; Salzmann, C.; Ongania, K.; De Biani, F. F.; Zanello, P.; Bildstein, B. *Organometallics* **2004**, *23*, 1024. (c) Hjelm, J.; Handel, R. W.; Hagfeldt, A.; Constable, E. C.; Housecroft, C. E.; Forster, R. J. *Inorg. Chem.* **2005**, *44*, 1073. (d) Constable, E. C.; Housecroft, C. E.; Neuburger, M.; Schaffner, S.; Shardlow, E. J. *Dalton Trans.* **2005**, *2*, 234.



Numerous studies on transition metal tpy-tpy complexes exhibiting luminescence from metal-to-ligand charge-transfer excited states have been reported. The complexes formed between 2,2':6',2''-terpyridine (tpy) and Ru^{2+} are normally only weakly luminescent at room temperature, but attaching a functionalized group at the 4'-position switches on the desired emission. It has been shown that a dinuclear Ru^{2+} complex of tpy-tpy substituted with an alkyne group at the 4'-position can possess a room-temperature luminescence lifetime ($\tau_p = 565$ ns) 1000-fold longer than that of a $Ru(tpy)_2^{2+}$ complex ($\tau_p = 0.56$ ns) in deoxygenated CH_3CN at 25 °C.¹³ Furthermore, the energy transfer along the molecular axis can be varied by incorporating additional groups into the alkyne spacer, and it has been shown that phenyl groups are especially effective at perturbing the electronic properties of the spacer.^{13,16,18}

Very recently, we have described²¹ the preparations of multinuclear supramolecules assembled from 1,1'-bis(terpyridyl)biferrocene redox-active subunits with Ru^{2+} metal centers (**1b**, Chart 2). The preparation of 4'-ferrocenyl-2,2':6',2''-terpyridine (fctpy) was reported previously,^{22,23} and cyclic voltammetric measurements of its Ru^{2+} metal complexes ($[Ru(tpy)(fctpy)]^{2+}$ and $[Ru(fctpy)_2]^{2+}$) indicated $Ru^{2+/3+}$ and ferrocenium/ferrocene



redox couples at ~ 1.3 and ~ 0.6 V vs Ag/AgCl, respectively.²⁴ In addition to the $\pi_{tpy} - \pi_{tpy}^*$ absorptions (240–280 nm) and the $d\pi_{Ru} - \pi_{tpy}^*$ MLCT absorption (~ 480 nm), the $[Ru(tpy)(fctpy)]^{2+}$ and $[Ru(fctpy)_2]^{2+}$ complexes exhibit an unusual $^1[(d(\pi)_{Fc})^6] \rightarrow ^1[(d(\pi)_{Fc})^5(\pi_{tpy}^*_{Ru})^1]$ MLCT absorption at ~ 510 nm.²⁴ The electrochemical measurements of the series of Ru^{2+} complexes of 1,1'-bis(terpyridyl)biferrocene are dominated by the Ru^{2+}/Ru^{3+} redox couple ($E_{1/2}$ at ~ 1.35 V), Fe^{2+}/Fe^{3+} redox couples ($E_{1/2}$ from ~ 0.4 to ~ 0.9 V), and tpy/tpy⁻/tpy²⁻ redox couples ($E_{1/2}$ at ~ -1.2 and ~ -1.4 V).²¹ The appreciable variations detected in the Fe^{2+}/Fe^{3+} oxidation potentials indicate that there is an interaction between the spacer and the Ru^{2+} metal centers. Coordination of Ru^{2+} metal centers to 1,1'-bis(terpyridyl)biferrocene results in a red-shifted and more intense $^1[(d(\pi)_{Fe})^6] \rightarrow ^1[(d(\pi)_{Fe})^5(\pi_{tpy}^*_{Ru})^1]$ transition in the visible region. The observed red-shifted absorption from ~ 510 nm in the monomeric $[Ru(tpy)(fctpy)]^{2+}$ complex to ~ 570 nm in polynuclear Ru^{2+} complexes of 1,1'-bis(terpyridyl)biferrocene reveals that there is a qualitative electronic coupling within the array.

In attempting to perturb the electronic properties of the spacer, we now describe the preparation and the physical properties of the tpy-(fc)_n-tpy (fc = ferrocene, $n = 1-3$) spacer containing redox-active moieties, and the coordination behavior with Ru^{2+} ions is also reported. Ferrocene is a delocalized π -electron ring system of an aromatic molecule. Furthermore, on the basis of the observation of the $^1[(d(\pi)_{Fc})^6] \rightarrow ^1[(d(\pi)_{Fc})^5(\pi_{tpy}^*_{Ru})^1]$ transition, the tpy-(fc)_n-tpy molecule appears to be a promising spacer that can ensure fast and quantitative transfer of energy within the array. Chart 2 shows the schematic structure of the Ru^{2+} complex of tpy-(fc)₃-tpy. The direct distances (16.0 Å with $n = 1$; 19.4 Å with $n = 2$; 25.2 Å with $n = 3$) between the two Ru^{2+} centers were estimated with the Spartan Mechanics Program (MMFF94). Our spectroscopic measurements in mixed-valence ferrocenium demonstrated that electron transfer in the biferrocenium system is quite facile.^{25,26} Ferrocene exhibits strong interactions between the metal orbitals and the π -system of the Cp rings, and electron delocal-

(15) Grosshenny, V.; Harriman, A.; Ziessel, R. *Angew. Chem., Int. Ed. Engl.* **1995**, *34*, 1100.

(16) El-ghayoury, A.; Harriman, A.; Khatyr, A.; Ziessel, R. *Angew. Chem., Int. Ed.* **2000**, *39*, 185.

(17) (a) Harriman, A.; Mayeux, A.; De Nicola, A.; Ziesel, R. *Phys. Chem. Chem. Phys.* **2002**, *4*, 2229. (b) Barbieri, A.; Ventura, B.; Barigletti, F.; De Nicola, A.; Quesada, M.; Ziessel, R. *Inorg. Chem.* **2004**, *43*, 7359. (c) Hjelm, J.; Handel, R. W.; Hagfeldt, A.; Constable, E. C.; Housecroft, C. E.; Forster, R. *J. Inorg. Chem.* **2005**, *44*, 1073.

(18) Hissler, M.; El-ghayoury, A.; Harriman, A.; Ziessel, R. *Angew. Chem., Int. Ed.* **1998**, *37*, 1717.

(19) Harriman, A.; Khatyr, A.; Ziessel, R.; Benniston, A. C. *Angew. Chem., Int. Ed.* **2000**, *39*, 4287.

(20) Barigletti, F.; Flamigni, L.; Calogero, G.; Hammarström, L.; Sauvage, J.-P.; Collin, J.-P. *J. Chem. Soc., Chem. Commun.* **1998**, 2333.

(21) Dong, T.-Y.; Lin, M. C.; Chiang, M. Y. N.; Wu, J. Y. *Organometallics* **2004**, *23*, 3921.

(22) Farlow, B.; Nile, T. A.; Walsh, J. L.; Mcphail, A. T. *Polyhedron* **1993**, *12*, 2891.

(23) Constable, E. C.; Edwards, A. J.; Martínez-Mañez, R.; Raithby, P. R.; Cargill Thompson, A. M. W. *J. Chem. Soc., Dalton Trans.* **1994**, 645.

(24) Hutchison, K.; Morris, J. C.; Nile, T. A.; Walsh, J. L.; Thompson, J. R.; Petersen, J. D.; Schoonover, J. R. *Inorg. Chem.* **1999**, *38*, 2516.

(25) Dong, T.-Y.; Chang, L. S.; Lee, G. H.; Peng, S. M. *Organometallics* **2002**, *21*, 4197, and references therein.

(26) Dong, T.-Y.; Chang, C. K.; Lee, S. H.; Lai, L. L.; Chiang, Y. N. M.; Lin, K. J. *Organometallics* **1997**, *16*, 5816.

ization could possibly be transmitted by metal–ligand orbital overlap. The present article describes the first step in the preparations of multinuclear complexes assembled from the redox-active molecules of tpy-(fc)_n-tpy attached to ruthenium(II) centers and concentrates on the spectroscopic properties of the simplest diruthenium complexes.

Experimental Section

General Information. All manipulations involving air-sensitive materials were carried out by using standard Schlenk techniques under an atmosphere of N₂. Solvents were dried as follows: THF and ether were distilled from Na/benzophenone; DMF and CH₂Cl₂ were distilled from CaH₂; TMEDA was distilled from KOH. Samples of 1-bromoferrocene-1'-carbaldehyde,²⁶ 1,1'-dibromoferrocene,²⁶ Ru(tpy)Cl₃,²⁷ *N*-[2-oxo-2-(2-pyridyl)ethyl]pyridinium iodide,²⁸ 1,1'-bis(terpyridyl)ferrocene,²⁹ and 1,1'-bis(terpyridyl)biferrocene (tpy-bifc-tpy)²¹ were prepared according to literature procedures. As shown in Schemes 1 and 2, complexes **1a–c** can be prepared.

Preparation of Triferrocene-1,1'-dicarbaldehyde (2c). A mixture of dibromoferrocene (1.17 g, 3.41 mmol) and 1-bromoferrocene-1'-carbaldehyde (2 g, 6.83 mmol) and activated copper (5 g) was heated under N₂ at 130–140 °C for 24 h. After cooling to room temperature, the reaction mixture was repeatedly extracted with CH₂Cl₂ until the extracts appeared colorless. The combined extracts were evaporated and chromatographed on neutral alumina (act. III). The first band eluting with hexane was the ferrocenes. The second band eluting with CH₂Cl₂/hexane (1:9) was biferrocene. The third band eluting with CH₂Cl₂/hexane (1:1) gave ferrocene-1-carbaldehyde. The fourth band eluting with EA/CH₂Cl₂ (1:99) was tetraferrocene-1,1'-dicarbaldehyde (2% yield). The last band eluting with EA (ethyl acetate)/CH₂Cl₂ (5:95) was triferrocene-1,1'-dicarbaldehyde (**2c**, 200 mg, 10% yield). The physical properties of tetraferrocene-1,1'-dicarbaldehyde are as follows. ¹H NMR (CDCl₃): δ 3.88 (t, 4H, *J* = 2 Hz, Cp), 3.94 (t, 4H, *J* = 2 Hz, Cp), 4.00 (s, 8H, Cp), 4.16 (t, 4H, *J* = 2 Hz, Cp), 4.21 (t, 4H, *J* = 2 Hz, Cp), 4.30 (t, 4H, *J* = 2 Hz, Cp), 4.48 (t, 4H, *J* = 2 Hz, Cp), 9.63 (s, 2H, CHO). MS (EI, 40 eV): M⁺ at *m/z* 794. Anal. Calcd for C₄₂H₃₄Fe₄O₂: C, 63.52; H, 4.32. Found: C, 63.50; H, 4.49. The physical properties of **2c** are as follows. ¹H NMR (CDCl₃): δ 4.08 (s, 8H, Cp), 4.20 (t, 4H, *J* = 2 Hz, Cp), 4.24 (t, 4H, *J* = 2 Hz, Cp), 4.34 (t, 4H, *J* = 2 Hz, Cp), 4.52 (t, 4H, *J* = 2 Hz, Cp), 9.68 (s, 2H, CHO). MS (EI, 40 eV): M⁺ at *m/z* 610. Anal. Calcd for C₄₂H₃₄Fe₄O₂: C, 62.99; H, 4.29. Found: C, 62.78; H, 4.61.

Preparation of Compound 3c. To a CH₂Cl₂ (10 mL) solution of **2c** (0.5 g, 0.8 mmol) was added a solution of 2-acetylpyridine (0.18 mL, 1.6 mmol) in ethanol (30 mL). The reaction mixture was stirred for 3 min, and then an aqueous solution (10 mL) of 2 M NaOH was added. After 30 min, the solution became dark violet and the reaction mixture was stirred at room temperature for 6 h. The ethanol solvent was removed under reduced pressure. The mixture was repeatedly extracted with CH₂Cl₂. The organic layer was dried over MgSO₄. After evaporation of the solvent, the crude product was chromatographed on Al₂O₃ (neutral, act. IV), eluting with hexane/CH₂Cl₂/EA (70/25/5). The first band was the desired compound. The yield was approximately 60%. The physical properties of **3c** are as follows. ¹H NMR (CDCl₃): δ 3.82 (t, 4H, *J* = 2 Hz, Cp), 3.93 (t, 4H, *J* = 2 Hz, Cp), 4.07 (t, 4H, *J* =

2 Hz, Cp), 4.11 (t, 4H, *J* = 2 Hz, Cp), 4.23 (t, 4H, *J* = 2 Hz, Cp), 4.36 (t, 4H, *J* = 2 Hz, Cp), 7.42 (ddd, 2H, *J* = 2 Hz, H₅), 7.54 (s, 4H, CH=CH), 7.82 (dt, 2H, *J* = 6 Hz, H₄), 8.12 (d, 2H, *J* = 9 Hz, H₃), 8.67 (d, 2H, *J* = 4 Hz, H₆). MS (FAB): M⁺ at *m/z* 816.

Preparation of 1,1'-Bis(terpyridyl)triferrocene (4c). To a solution of **3c** (0.4 g, 0.49 mmol) in CH₂Cl₂ (5 mL) was added an ethanol solution (50 mL) of ammonium acetate (~3 g) and *N*-[2-oxo-2-(2-pyridyl)ethyl]pyridinium iodide (0.32 g). The reaction mixture was heated under reflux for 5 h. The solution became dark red, and the ethanol solvent was removed under reduced pressure after cooling to room temperature. The mixture was repeatedly extracted with CH₂Cl₂. The organic layer was dried over MgSO₄. After evaporation of the solvent, the crude product was chromatographed on Al₂O₃ (neutral, act. IV), eluting with hexane/CH₂Cl₂ (50/50). The first band was the desired compound. The yield was approximately 20%. The product was recrystallized from CH₂Cl₂/ether (1:5). The physical properties of **4c** are as follows. ¹H NMR (CDCl₃): δ 3.54 (t, 4H, *J* = 2 Hz, Cp), 3.69 (t, 4H, *J* = 2 Hz, Cp), 3.96 (s, 8H, *J* = 2 Hz, Cp), 4.19 (t, 4H, *J* = 2 Hz, Cp), 4.70 (t, 4H, *J* = 2 Hz, Cp), 7.30 (dt, 4H, *J* = 5.5 Hz, H_{5,5'}), 7.81 (dt, 4H, *J* = 7.5 Hz, H_{4,4''}), 8.15 (s, 4H, H_{3,3'}), 8.56 (d, 4H, *J* = 8 Hz, H_{3,3''}), 8.67 (d, 4H, *J* = 4 Hz, H_{6,6''}). MS (FAB): M⁺ at *m/z* 1017. Anal. Calcd for C₆₀H₄₄N₆Fe₃: C, 70.89; H, 4.36; N, 8.27. Found: C, 70.59; H, 4.43; N, 7.81. Mp: 226–228 °C.

Preparation of Ru²⁺ Complex 1a. Under a nitrogen atmosphere, AgBF₄ (130 mg, 0.67 mmol) in 50 mL of ethanol was added to a solution of Ru(tpy)Cl₃ (67 mg, 0.14 mmol) in ethanol, and the mixture was heated to reflux for 12 h. The mixture was filtered under nitrogen. The filtrate was added to a solution of **4a** (45 mg, 0.07 mmol) which contained 10 drops of N(C₂H₅)₃, and the solution was refluxed for 24 h under a nitrogen atmosphere. After cooling, the volume of ethanol solvent was reduced to one-half, and then NH₄PF₆ (228 mg, 1.4 mmol) was added to give a violet-red precipitate. After cooling at 0 °C for 10 min, the precipitate was collected by filtration. The product was dissolved in acetone and purified by chromatography on act. V Al₂O₃, eluting with CH₃CN/CH₂Cl₂ (9:1). The third band was the desired compound. The product was recrystallized from CH₃CN/ether. The yield of **1a** was ~8%. ¹H NMR (*d*₆-acetone) of **1a**: δ 4.90 (s, 4H, Cp), 5.57 (s, 4H, Cp), 7.11 (t, 4H, *J* = 7.0 Hz, tpy-H_{5,5''}), 7.25 (t, 4H, *J* = 7.0 Hz, cp-tpy-H_{5,5''}), 7.33 (d, 4H, *J* = 5.0 Hz, tpy-H_{6,6''}), 7.53 (d, 4H, *J* = 5.5 Hz, cp-tpy-H_{6,6''}), 7.70 (t, 4H, *J* = 8.0 Hz, tpy-H_{4,4''}), 7.94 (t, 4H, *J* = 7.5 Hz, cp-tpy-H_{4,4''}), 8.41 (t, 2H, *J* = 8.5 Hz, tpy-H_{4'}), 8.52 (d, 4H, *J* = 7.5 Hz, cp-tpy-H_{3,3''}), 8.57 (d, 4H, *J* = 8.0 Hz, tpy-H_{3,3''}), 8.76 (d, 4H, *J* = 8.5 Hz, tpy-H_{5,5''}), 8.82 (s, 4H, cp-tpy-H₅). MS of **1a** (FAB): [M – PF₆]⁺ *m/z* at 1751; [M – 2PF₆]⁺ *m/z* at 1606. Anal. Calcd for **1a**·5H₂O (C₇₀H₆₀F₂₄FeN₁₂O₅P₄Ru₂): C, 42.31; H, 3.04; N, 8.46. Found: C, 42.13; H, 3.20; N, 8.56.

Preparation of Ru²⁺ Complex 1c. An ethanol (50 mL) solution of **4c** (0.0315 mmol), a stoichiometric amount of Ru(tpy)Cl₃, and 10 drops of N(C₂H₅)₃ were heated to reflux for 8 h. After cooling the reaction mixture, the volume of ethanol solvent was reduced to one-half. An aqueous solution of NH₄PF₆ was added to give a violet-red precipitate, which was collected by filtration. The crude product was chromatographed on act. V Al₂O₃, eluting with hexane/acetone (1:1). Elution with acetone afforded compound **1c**. The yield of **1c** was ~30%. ¹H NMR (*d*₆-acetone) of **1c**: δ 3.54 (dd, 4H, Cp), 4.26 (dd, 4H, Cp), 4.32 (dd, 4H, Cp), 4.53 (dd, 4H, Cp), 4.60 (dd, 4H, Cp), 5.25 (dd, 4H, Cp), 7.24 (t, 4H, *J* = 6.0 Hz, tpy-H_{5,5''}), 7.27 (t, 4H, *J* = 6.0 Hz, cp-tpy-H_{5,5''}), 7.57 (d, 4H, *J* = 5.5 Hz, tpy-H_{6,6''}), 7.65 (d, 4H, *J* = 5.5 Hz, cp-tpy-H_{6,6''}), 8.01 (t, 4H, *J* = 7.5 Hz, tpy-H_{4,4''}), 8.08 (t, 4H, *J* = 7.5 Hz, cp-tpy-H_{4,4''}), 8.54 (t, 2H, *J* = 8.0 Hz, tpy-H_{4'}), 8.61 (s, 4H, cp-tpy-H₅), 8.68 (d, 4H, *J* = 8.0 Hz, tpy-H_{3,3''}), 8.79 (d, 4H, *J* = 8.0 Hz, cp-tpy-H_{3,3''}), 9.05 (d, 4H, *J* = 8.0 Hz, tpy-H₅). MS of **1c** (ESI): [M – 2PF₆]²⁺ *m/z* at 987; [M – 3PF₆]³⁺ *m/z* at 610; [M – 4PF₆]⁴⁺

(27) Sullivan, B. P.; Calvert, J. M.; Meyer, T. *Inorg. Chem.* **1980**, *19*, 1404.

(28) Priimov, G. U.; Moore, P.; Maritim, P. K.; Butalanyi, P. K.; Alcock, N. W. *J. Chem. Soc., Dalton Trans.* **2000**, 445.

(29) Constable, E. C.; Edwards, A. J.; Marcos, M. D.; Raithby, P. R.; Martínez-Mañez, R.; Tendero, M. J. L. *Inorg. Chim. Acta* **1994**, *224*, 11.

Table 1. Experimental and Crystal Data for **4c**

formula	C ₆₀ H ₄₄ Fe ₃ N ₆
<i>M_w</i>	1016.56
cryst syst	monoclinic
space group	<i>P</i> 2 ₁ / <i>n</i>
<i>a</i> (Å)	11.8300(2)
<i>b</i> (Å)	21.3310(3)
<i>c</i> (Å)	19.0910(4)
β (deg)	105.618(1)
<i>V</i> (Å ³)	4639.7(1)
<i>Z</i>	4
<i>d</i> _{calcd} (g cm ⁻³)	1.455
μ (mm ⁻¹)	0.975
λ (Å)	0.71073
2θ limits (deg)	55
transmn coeff	0.782–0.871
R1 ^a	0.0444
wR2 ^b	0.1002

^a R1 = $\sum ||F_o|| - ||F_c|| / \sum ||F_o||$. ^b wR2 = $[(\sum w(F_o^2 - F_c^2)^2) / (\sum wF_o^2)^2]^{1/2}$.

m/z at 421. Anal. Calcd of **1c** (C₉₀H₆₆F₂₄Fe₃N₁₂P₄Ru₂): C, 47.72; H, 2.94; N, 7.42. Found: C, 47.62; H, 3.24; N, 7.18.

Physical Methods. ¹H NMR spectra were run on a Varian INOVA-500 MHz spectrometer. Mass spectra were obtained with a VG-BLOTECH-QUATTRO 5022 system, and ESI-LCQ mass spectra were obtained with a Thermo Finnigan spectrometer. UV spectra were recorded from 250 to 800 nm in CH₃CN by using 1.0 cm quartz cells with a Hitachi U-4001 spectrophotometer. Electrochemical measurements were carried out with a BAS 100W system. Cyclic voltammetry was performed with a stationary glassy carbon working electrode. These experiments were carried out with a 1 × 10⁻³ M solution of CH₂Cl₂/CH₃CN (1:1) containing 0.1 M of (*n*-C₄H₉)₄NPF₆ as supporting electrolyte. The potentials quoted in this work are relative to a Ag/AgCl electrode at 25 °C. Under these conditions, ferrocene shows a reversible one-electron redox wave (*E*_{1/2} = 0.46 V).

Structure Determination of 4c. A red crystal (0.25 × 0.20 × 0.10 mm) was grown when a layer of ether was allowed to slowly diffuse into a CH₂Cl₂ solution of **4c**. The single-crystal X-ray determination of compound **4c** with Mo Kα radiation was carried out at 298 K by using an Enraf Nonius CAD4 diffractometer. Data were collected to a maximum 2θ value of 55.0°. Of the 10 622 unique reflections (*R*_{int} = 0.0535) collected, there were 10 490 with *F*_o² > 2.0σ(*F*_o²). An empirical absorption correction based on azimuthal scans of several reflections was applied. The structures were solved by an expanded Fourier technique. All non-hydrogen atoms were refined anisotropically. Hydrogen atoms were included at ideal distance (1.08 Å). The X-ray crystal data are summarized in Tables 1 and 2. Complete tables of the final positional parameters for all atoms, the bond distances and angles, and thermal parameters of compound **4c** are given in the Supporting Information.

Results and Discussion

Molecular Structure of 4c. Details of the X-ray crystal data collections and unit-cell parameters are given in Table 1. The molecular structure of **4c** is shown in Figure 1, and selected bond distances and angles are given in Table 2. Complete tables of positional parameters, bond distances, and bond angles are given as Supporting Information.

As shown in Figure 1, the ORTEP view confirms the molecular structure with the triferrocenyl group directly linked to the 4'-position of the 2,2':6',2''-terpyridine. The triferrocenyl moiety exists in a trans conformation with the two iron ions on opposite sides of the fulvalene ligand in which the two Cp rings form dihedral angles of 2.6(3)° and 2.6(3)°. A direct comparison was made for

Table 2. Selected Bond Distances and Angles for **4c**

Distance (Å)			
Fe(1)–C(1)	2.046(3)	Fe(3)–C(21)	2.072(2)
Fe(1)–C(2)	2.045(3)	Fe(3)–C(22)	2.043(3)
Fe(1)–C(3)	2.041(3)	Fe(3)–C(23)	2.027(3)
Fe(1)–C(4)	2.028(4)	Fe(3)–C(24)	2.035(3)
Fe(1)–C(5)	2.031(3)	Fe(3)–C(25)	2.044(3)
Fe(1)–C(6)	2.062(2)	Fe(3)–C(26)	2.038(3)
Fe(1)–C(7)	2.041(3)	Fe(3)–C(27)	2.037(3)
Fe(1)–C(8)	2.029(3)	Fe(3)–C(28)	2.038(3)
Fe(1)–C(9)	2.030(4)	Fe(3)–C(29)	2.048(3)
Fe(1)–C(10)	2.034(3)	Fe(3)–C(30)	2.047(3)
Fe(2)–C(11)	2.067(3)	C(16)–C(31)	1.476(3)
Fe(2)–C(12)	2.045(3)	C(33)–C(36)	1.490(4)
Fe(2)–C(13)	2.035(3)	C(34)–C(41)	1.493(4)
Fe(2)–C(14)	2.034(3)	C(26)–C(46)	1.478(4)
Fe(2)–C(15)	2.045(3)	C(49)–C(51)	1.491(5)
Fe(2)–C(16)	2.046(3)	C(48)–C(56)	1.484(5)
Fe(2)–C(17)	2.046(3)		
Fe(2)–C(18)	2.052(3)		
Fe(2)–C(19)	2.040(3)		
Fe(2)–C(20)	2.041(3)		
Angles (deg)			
C(32)–C(31)–C(35)	117.6(2)	C(50)–C(46)–C(47)	116.9(3)
C(33)–N(1)–C(34)	117.4(2)	C(48)–N(4)–C(49)	118.2(3)
C(37)–N(2)–C(36)	117.0(3)	C(51)–N(5)–C(55)	117.7(4)
C(41)–N(3)–C(45)	117.5(3)	C(56)–N(6)–C(57)	117.9(4)

fctpy, tpy-fc-tpy (**4a**), bific-tpy, tpy-bific-tpy (**4b**), and tpy-trifc-tpy (**4c**) (Table 3). Inspection of the average distances of Fe–C and Fe–Cp (Fe1–C, 2.038(3); Fe1–Cp, 1.646(2); Fe2–C, 2.045(3); Fe2–Cp, 1.652(2); Fe3–C, 2.042(3); Fe3–Cp, 1.649(2) Å) indicates that the three metallocenes are in the Fe²⁺ oxidation state. The bonds and angles about the Cp rings vary little, and they are close to those reported for analogous ferrocenes.²⁶ The two Cp rings associated with Fe1, Fe2, and Fe3 are nearly parallel, and the dihedral angles are 2.6(3)°, 2.6(3)°, and 1.0(2)°, respectively. Furthermore, the two Cp rings associated with Fe1 and Fe3 are staggered, with average staggering angles of 16.3° and 12.3°, respec-

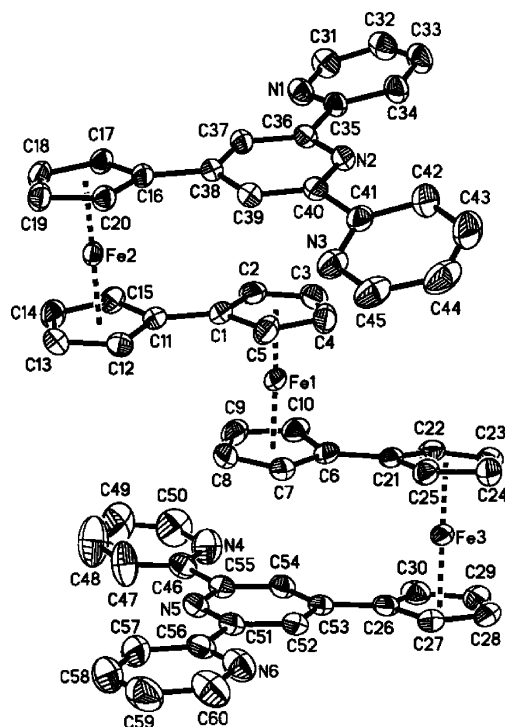
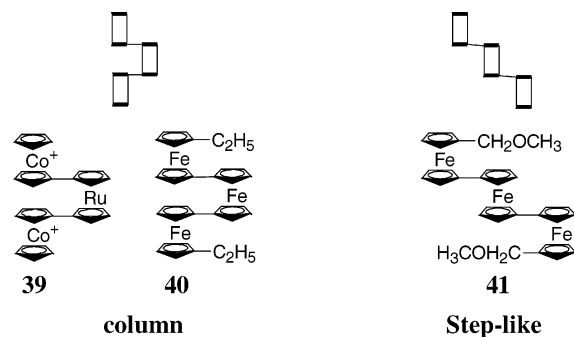
Figure 1. ORTEP drawing for **4c**.

Table 3. Comparison of the Atomic Distances and Angles

	4c	tpy-bifc ⁱ	4bⁱ	4aⁱ	tpy-fe ^k
Fe1–C ^a	2.038(3)	2.043(5)	2.035(6)	2.042(9)	2.044(3)
Fe2–C ^a	2.045(3)		2.030(7)		
Fe3–C ^a	2.042(3)				
Fe1–Cp ^b	1.646(2)	1.65	1.642		
Fe2–Cp ^b	1.652(2)		1.651		
Fe3–Cp ^b	1.649(2)				
ta(Fe1) ^c	2.61(0.27)				
ta(Fe2) ^c	2.58(0.26)				
ta(Fe3) ^c	1.02(0.23)				
sa(Fe1) ^d	16.3	15.5	18.45		
sa(Fe2) ^d	2.0		24.90		
sa(Fe3) ^d	12.3				
C–C(py) ^e	1.375(5)	1.392(5)	1.394(4)	1.376(13)	1.384(10)
C–N(py) ^f	1.335(4)	1.340(5)	1.329(6)	1.337(10)	1.342(2)
da(Cp-py) ^g	9.31(0.21)	11.87	16.09	6.0	19.2
	4.8(0.21)				
da(py-py) ^h	11.52–15.33	9.18–14.52	4.43–6.37	2.7–10.5	7.3
	2.97–5.66				

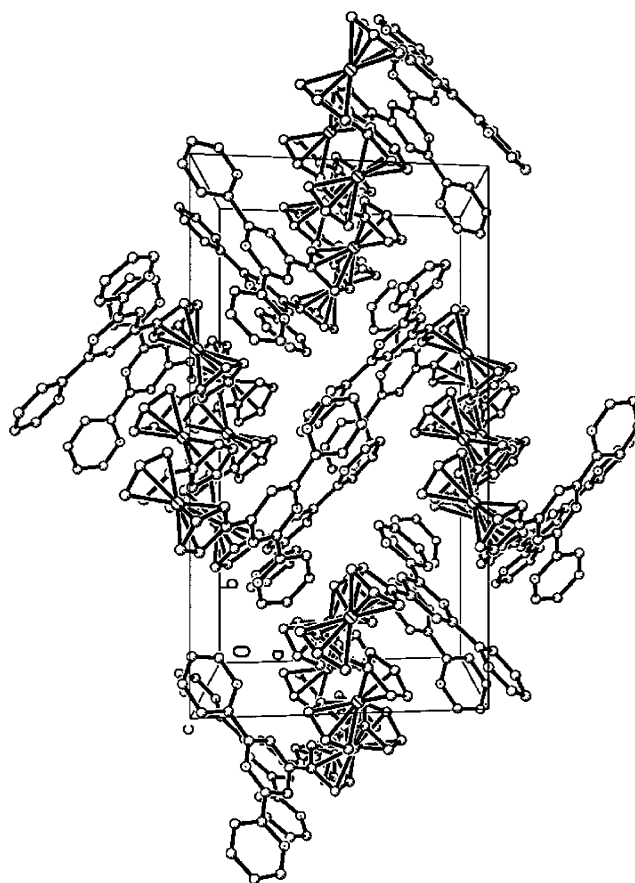
^a Average Fe–C distance for each ferrocenyl moiety. ^b Distance from the Fe atom to the center of mass of the Cp ring in each ferrocenyl moiety. ^c Dihedral angle between the two least-squares-fitting Cp ring in each ferrocenyl moiety. ^d Average stagger angle between the two Cp rings in each ferrocenyl moiety. ^e Average C–C distance in the pyridine rings. ^f Average C–N in the pyridine rings. ^g Dihedral angle between the Cp ring and the central ring of the terpyridine moiety. ^h Dihedral angle between the central ring and the terminal ring for each terpyridine moiety. ⁱ From ref 21. ^j From ref 29. ^k From ref 22.

Chart 3

tively. However, the two Cp rings associated with Fe2 are nearly eclipsed, with an average staggering angle of 2.0°. Attachment of a tpy moiety to the 1'-position of triferrocene has minimal influence on the molecular structure in comparison with analogous triferrocene.³⁰

The 2,2':6', 2''-terpyridine group adopts the expected trans–trans conformation about the interannular C33–C36 and C34–C41 bonds.^{29,31} As given in Table 3, the pyridyl units in each terpyridine group are not completely coplanar. The directly bonded Cp ring of the ferrocene group is also not coplanar with the central pyridyl ring of terpyridine.

The two tpy substituents in **4c** show a cisoid conformation relative to the fulvalenide ligand. The molecular structure of **4c** can be described as steplike with regard to the ferrocenyl moieties. As shown in Chart 3, two types (steplike and column) of molecular structures have been observed in other triferrocenyl compounds.^{30,32} In the case of steplike **4c**, there is no intramolecular Cp–Cp π – π interaction; however, a significant intramolecular π – π interaction (3.3(2) Å) between the Cp ring of the central ferrocenyl moiety and the central pyridyl ring of the terpyridyl group is observed. From the

**Figure 2.** Stereopacking arrangement of **4c**.

packing arrangement (Figure 2), there is no Cp–Cp or Cp–Py interaction between neighboring molecules in the solid-state structure.

Electrochemical Results of Free Ligand 4. Electrochemical data for the free bis(terpyridyl)ferrocenes (**4a–c**), as well as those for some other relevant compounds, are shown in Table 4. Compounds **4a–c** show successive reversible one-electron oxidations. Electrochemical reversibility is demonstrated by the peak-to-peak separation (ΔE_p in Table 4) between the resolved

(30) Dong, T.-Y.; Lee, W. Y.; Su, P. T.; Chang, L. S.; Lin, K. J. *J. Organometallics* **1998**, *17*, 3323.

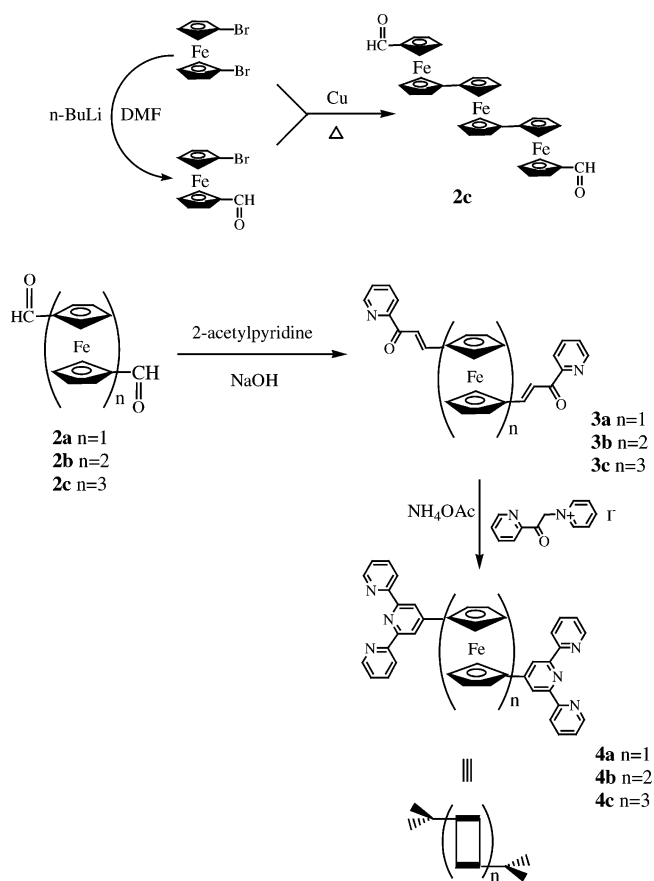
(31) Sasaki, I.; Daran, J. C.; Ait-Haddou, H.; Balavoine, G. G. A. *Inorg. Chem. Commun.* **1998**, *1*, 354.

(32) Jaitner, P.; Schottenberger, H.; Gamper, S.; Obendorf, D. *J. Organomet. Chem.* **1994**, *475*, 113.

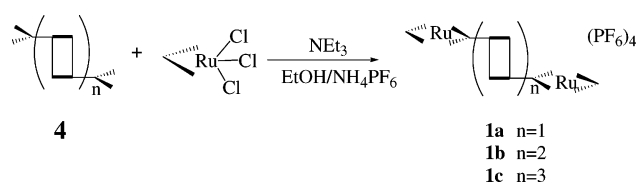
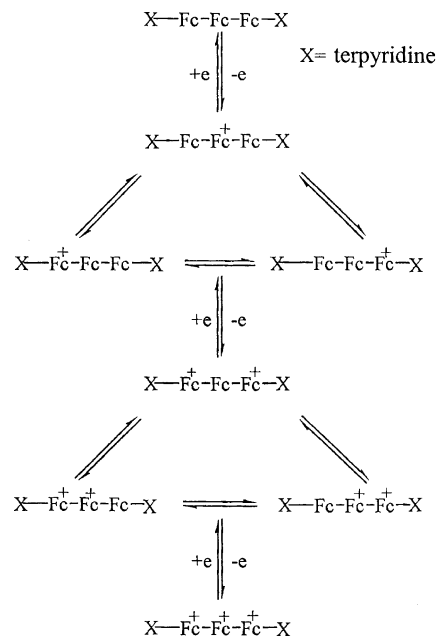
Table 4. Cyclic Voltammetry for Various Neutral Ferrocenes

compound	$E_{1/2}$ (V) ^a	$\Delta E_{1/2}$ (V) ^b	ΔE_p (mV) ^c	I_a/I_c ^d	$10^{-5} \times K_c$ ^e
ferrocene	0.46		70	1.03	
biferrocene ^f	0.37	0.32	70	1.01	2.65
	0.71		75	1.01	
triferrocene ^g	0.28	0.22			0.0536
	0.50	0.38			27.6
	0.88				
fc-tpy ^f	0.63				
bifc-tpy ^f	0.45	0.45	80	1.01	423
	0.90		76	0.93	
4a	0.70		70	2.11	
4b^f	0.51	0.43	72	1.07	194
	0.94		73	1.13	
4c	0.37	0.40	80	0.57	60.2
	0.77	0.27	60	0.81	0.377
	1.04		64	1.18	

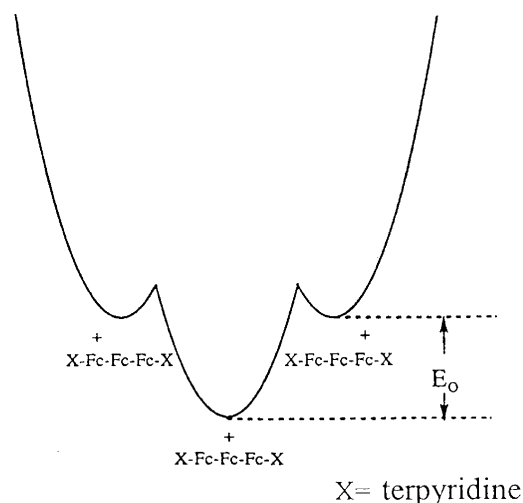
^a All half-wave potentials are referenced to the Ag/AgCl electrode in CH₂Cl₂/CH₃CN (1:1) solution. ^b The difference of $E_{1/2}$ between two redox waves. ^c Peak-to-peak separation between the resolved reduction and oxidation wave maxima. ^d Peak-current ratio between cathode and anode. ^e Comproportionation equilibrium constant. ^f From ref 21. ^g From ref 30.

Scheme 1

reduction and oxidation wave maxima. In fact, ΔE_p is larger than the theoretical value of 59 mV. Under our experimental conditions, the ferrocene-ferrocenium couple has $\Delta E_p = 70$ mV, which is used as the criterion for reversibility. The effect of terpyridyl substituents on the stability of the Fe³⁺ state is illustrated by the shift of half-wave potentials. The comparison of the half-wave potentials of **4** with corresponding ferrocenes indicates that the terpyridyl substituent acts as a net electron-withdrawing group.³⁰

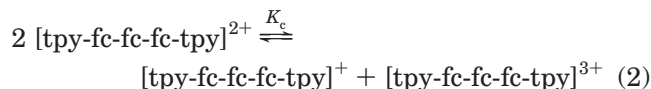
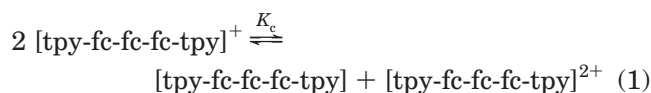
Scheme 2**Scheme 3**

For compound **4c**, there are two chemically different oxidation-reduction sites (tpy-fc- and -fc-). Upon oxidation-reduction to the mixed-valence ions, more than one oxidation isomer can exist (Scheme 3). Furthermore, the isomers may differ in free energy. For example, the monocation of **4c** can exist as one of two energetically equivalent isomers, tpy-fc⁺-fc-fc-tpy and tpy-fc-fc-fc⁺-tpy, or as the energetically nonequivalent isomer tpy-fc-fc⁺-fc-tpy (Figure 3). The distribution between the various isomers depends on the zero-point energy difference (E_0) between them. We believe that the nature of the substituent has direct influence on the magnitude of E_0 .

**Figure 3.** Potential energy-configuration diagram for the monocation of **4c**.


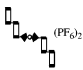
The value of E_0 is a result of the electronic effects of the tpy substituents and the ferrocenyl moieties. It is important to realize that energetically it is the tpy- fc^+ - fc -tpy energy surface destabilized more by the electron-withdrawing tpy substituent. Furthermore, the stabilization in the tpy- fc - fc^+ - fc -tpy energy surface by the electron-releasing ferrocenyl moieties is expected. In the case of the dication, the repulsion between the ferrocenium cations results in the difficulty in estimating the energy surfaces for tpy- fc^+ - fc^+ - fc -tpy, tpy- fc - fc^+ - fc^+ -tpy, and tpy- fc^+ - fc - fc^+ -tpy oxidation isomers.

One of the interesting attributes of **4b,c** is the magnitude of the electronic interaction between the three Fe sites. Cyclic voltammetry affords a simple and effective way for estimating this interaction. It has been demonstrated that the magnitude of the peak-to-peak separation ($\Delta E_{1/2}$) gives an indication of the interaction between the metal sites in the solution state.³³ A comparison of the magnitude of $\Delta E_{1/2}$ between triferrocene and **4c** indicates that the magnitude of the interaction between the Fe sites in the *solution state* in **4c** is greater than that in triferrocene. This indicates that the interaction between the Fe sites is sensitive to the nature of the terpyridyl substituent. This observation has also been seen in a comparison of the $\Delta E_{1/2}$ values of tpy-bifc-tpy and biferrocene.²¹ As shown in Table 4, the disproportionation constants K_c of eqs 1 and 2 can be calculated from the values of $\Delta E_{1/2}$.



Electrochemical Results of Ru²⁺ Complexes (1a–c). The electrochemical parameters for **1** and related compounds obtained from the CV are summarized in Table 5. As expected, the redox behavior of **1** is dominated by the Ru²⁺/Ru³⁺ redox couple ($E_{1/2}$ from 1.35 to 1.38V), Fe²⁺/Fe³⁺ redox couples ($E_{1/2}$ from 0.4 to 1.0 V), and tpy/tpy⁻/tpy²⁻ redox couples ($E_{1/2}$ from -1.3 to -1.5 V). To show the Fe²⁺/Fe³⁺ and tpy/tpy⁻/tpy²⁻ redox couples, the CV voltammograms of **1a–c** are shown in Figure 4 in the range from +1.2 to -1.7 V with a scan rate of 100 mV s⁻¹. As shown in Figure 4, complexes **1a–c** show reversible oxidation processes on sweeping at anodic potentials, corresponding to the oxidation of the ferrocenyl moieties. Furthermore, two consecutive reduction waves attributed to the reduction of the Ru(tpy)₂²⁺ core are also observed. The smaller $\Delta E_{1/2}$ values in **1b,c** (0.31 V for **1b**; 0.31 and 0.26 V for **1c**) in comparison with corresponding neutral free ligands **4b,c** are expected on the basis of charge buildup after the coordination of the Ru²⁺ ion. A comparison of the values of $\Delta E_{1/2}$ between **1b** and **1c** indicates that the magnitude

Table 5. CV Data of **1** and Related Compounds with a Scan Rate of 100 mV s⁻¹

compd	Ru-center		Fe-center		TPy-center
	$E_{1/2}$ (V) ^a	$E_{1/2}$ (V) ^a	$\Delta E_{1/2}$ (V) ^b	$E_{1/2}$ (V) ^a	
[Ru(tpy) ₂] ²⁺ , ^c	1.27			-1.27	
 (PF ₆) ₂	1.36	0.48	0.40	-1.16	
		0.88		-1.43	
 (PF ₆) ₂	1.35	0.49	0.39	-1.20	
		0.88		-1.45	
1a	1.38	0.80		-1.17	
				-1.42	
1b	1.35	0.61	0.31	-1.18	
		0.92		-1.42	
1c	1.35	0.41	0.31	-1.21	
		0.72	0.26	-1.46	
		0.98			

^a All half-wave potentials are referenced to the Ag/AgCl electrode in CH₂Cl₂/CH₃CN (1:1) solution. ^b The difference of $E_{1/2}$ between two redox waves. ^c From ref 17.

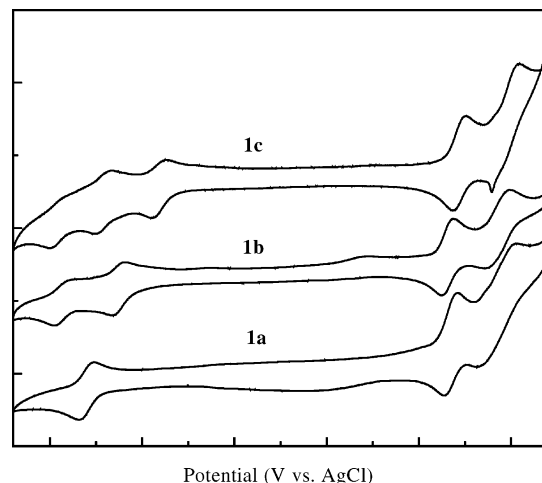


Figure 4. Cyclic voltammograms of Ru²⁺ complexes **1a–c**.

of interaction between the Fe sites in both complexes is similar in the solution state.

Attachment of ferrocenyl moieties to the 4'-position of tpy in Ru²⁺ complexes has minimal influence on the Ru²⁺/Ru³⁺ redox potential (from 1.35 to 1.38 V). These Ru²⁺-centered oxidation processes are more positive by at least 80 mV compared to those of [Ru(tpy)₂]²⁺. For the binuclear Ru²⁺ complexes of tpy-(fc)_n-tpy, a single wave is found for the Ru²⁺/Ru³⁺ redox couple, a fact that might indicate that the electronic coupling between the Ru²⁺ centers is relatively weak. Very recently, the physical properties of a series of linearly arranged Ru²⁺ complexes, [(tpy)Ru(tpy-(DEDBT)_n-tpy)Ru(tpy)]⁴⁺ $n = 1, 2, 3, 4, 5$, featuring Ru²⁺-tpy chromophores connected to π -conjugated organic 2,5-diethynyl-3,4-dibutylthiophene oligomeric fragments (DEDBT), have been reported.¹⁷ The distance between two chromophoric centers was estimated from 18.5 Å ($n = 1$) to 42 Å ($n = 5$). In these diethynyl-thiophene-bridged complexes, a single

(33) (a) Atzkern, H.; Huber, B.; Köhler, F. H.; Müller, G.; Müller, R. *Organometallics* **1991**, *10*, 238. (b) Bunel, E. E.; Campos, P.; Ruz, P.; Valle, L.; Chadwick, I.; Ana, M. S.; Gonzalez, G.; Manriquez, J. M. *Organometallics* **1988**, *7*, 474. (c) Cowan, D. O.; Shu, P.; Hedberg, F. L.; Rossi, M.; Kistenmacher, T. J. *J. Am. Chem. Soc.* **1979**, *101*, 1304. (d) Moulton, R.; Weidman, T. W.; Vollhardt, K. P. C.; Bard, A. J. *Inorg. Chem.* **1986**, *25*, 1846. (e) Obendorf, D.; Schottenberger, H.; Rieker, C. *Organometallics* **1991**, *10*, 1293.

Table 6. UV–Visible Absorption Data^a

compound	absorption data, λ_{\max} , nm (ϵ , $\times 10^{-3} \text{ M}^{-1} \text{ cm}^{-1}$)
ferrocene	437(96), 322(56)
biferrocene	450(0.57), 296(7.90), 269(8.46)
triferrocene	465(1.9), 304(15), 220(65)
terpyridine	278
fctpy	459(0.91), 364(2.2), 280(28), 248(28)
bifc-tpy	460(1.3), 355(sh), 285(27), 274(29), 258(43)
4a	462(0.3), 370(1.3), 306(sh), 275(15), 247(19)
4b	481(4.3), 340(sh), 281(99), 276(104), 272(99), 253(130)
4c	468(2.6), 310(sh), 275(44), 250(47)
[Ru(tpy) ₂][PF ₆] ₂ ^b	517(4.2), 472(14), 435(7.9), 308(51), 270(36)
[Ru(tpy)(fctpy)][PF ₆] ₂ ^c	515 (sh), 478(15), 306(61), 270(41)
[Ru(fctpy) ₂][PF ₆] ₂ ^c	526(15), 482(15), 310(60), 284(44), 274(49)
1a	546(14), 519(21), 485(31), 443(18), 307(113), 273(94)
1b	555(20), 525(28), 482(53), 438(30), 308(200), 270(174)
1c	559(14), 526(18), 480(29), 437(17), 310(120), 273(82)

^a Acetonitrile solution at room temperature. ^b This work. ^c See ref 24.

wave of the Ru²⁺/Ru³⁺ redox couple was also found at ~1.36 V. The electronic coupling between the Ru²⁺ centers in the tpy-DEDBT-tpy system is also relatively weak. However, in our case there were appreciable variations detected in the potentials associated with the Fe²⁺/Fe³⁺ redox couples in complexes **1a–c**. The variations of the $\Delta E_{1/2}$ values (0.40 and 0.27 V in free ligand **4c** and 0.31 and 0.26 V in its Ru²⁺ complex (**1c**); 0.43 V in tpy-bifc-tpy (**4b**) and 0.31 V in its Ru²⁺ complex (**1b**)) and the appreciable variations detected in the Fe²⁺/Fe³⁺ oxidation potentials strongly suggest that there is an interaction between the spacer and the Ru²⁺ centers. The positive potential shift of the $E_{1/2}$ values for the Fe²⁺/Fe³⁺ redox couples upon the coordination of the Ru²⁺ ion with a free ligand indicates that there is an interaction between Ru²⁺ and Fe²⁺ centers. Thus, the ferrocenyl spacer plays a more sensitive role to gauge the interaction between the Ru²⁺ and Fe²⁺ centers. This is possible due to the existence of weak back-bonding of the Fe²⁺ metal center to the tpy ligand. Furthermore, the decreasing of $\Delta E_{1/2}$ values indicates that the magnitude of the Fe–Fe interaction is changed pronouncedly on the coordination of the Ru²⁺ ion. The smaller value of $\Delta E_{1/2}$ gives an indication of the smaller Fe–Fe interaction.

UV–Visible Spectroscopy. The UV–visible spectral data of **1**, **4**, and relevant compounds are summarized in Table 6. As shown in Figure 5, transitions occurring in the UV region ($\lambda < 350$ nm) are ascribed to the ligand-localized nature, mainly of tpy origin, of both the free ligand and coordinated tpy fragments. The visible absorption bands at 325 nm ($\epsilon = 51 \text{ M}^{-1} \text{ cm}^{-1}$) and 440 nm ($\epsilon = 87 \text{ M}^{-1} \text{ cm}^{-1}$) of ferrocene have been assigned to the $^1A_{1g} \rightarrow ^1E_{1g}$ and $^1A_{1g} \rightarrow ^1E_{2g}$ d–d transitions, respectively.^{34–36} In comparison with ferrocene, the $^1A_{1g}$

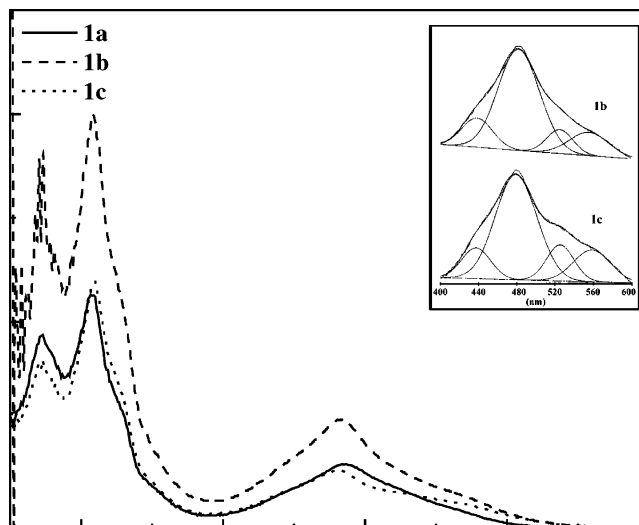


Figure 5. UV–visible absorption spectra of Ru²⁺ complexes **1a–c**. Inset: computer deconvolution for **1b** and **1c**.

$\rightarrow ^1E_{2g}$ d–d transitions of biferrocene (450 nm, $\epsilon = 570 \text{ M}^{-1} \text{ cm}^{-1}$) and triferrocene (465 nm, $\epsilon = 1900 \text{ M}^{-1} \text{ cm}^{-1}$) are red-shifted, and the molar absorptivity is considerably enhanced. Attachment of tpy to the ferrocenyl moiety has a significant influence on the d–d transition. The absorption bands for **4b** (481 nm, $\epsilon = 4300 \text{ M}^{-1} \text{ cm}^{-1}$) and **4c** (468 nm, $\epsilon = 2600 \text{ M}^{-1} \text{ cm}^{-1}$) are red-shifted relative to the biferrocene and triferrocene, and the molar absorptivities scale with the number of tpy substituents, consistent with the electron-withdrawing character of tpy.^{35,36}

As shown in Table 6, the visible spectra for Ru²⁺ complexes are also dominated by $^1[(d(\pi)_{\text{Ru}})^6] \rightarrow ^1[d(\pi)^5(\pi^*_{\text{tpy}})^1]$ MLCT absorption bands at ~480 nm, which were assigned by analogy to the well-documented MLCT transitions found for [Ru(tpy)₂]²⁺ (472 nm; $\epsilon = 14\,000 \text{ M}^{-1} \text{ cm}^{-1}$), [Ru(tpy)(fctpy)]²⁺ (478 nm; $\epsilon = 15\,000 \text{ M}^{-1} \text{ cm}^{-1}$), and [Ru(fctpy)₂]²⁺ (482 nm, $\epsilon = 15\,000 \text{ M}^{-1} \text{ cm}^{-1}$).^{24,37–39} The MLCT bands at 485 nm ($\epsilon = 31\,000 \text{ M}^{-1} \text{ cm}^{-1}$) for **1a**, at 482 nm ($\epsilon = 53\,000 \text{ M}^{-1} \text{ cm}^{-1}$) for **1b**, and at 480 nm ($\epsilon = 29\,000 \text{ M}^{-1} \text{ cm}^{-1}$) for **1c** are slightly red-shifted relative to the monomeric Ru-coordinated compounds, and the molar absorptivities are considerably enhanced. The absorption bands are broad because they include a series of MLCT transitions. Computer deconvolution of the MLCT band with three Gaussian lines was carried out. The resulting fitting curves are collected in Table 6 and shown in Figure 5. Well-defined shoulders on the $^1[(d(\pi)_{\text{Ru}})^6] \rightarrow ^1[d(\pi)^5(\pi^*_{\text{tpy}})^1]$ MLCT band are observed for the monomeric [Ru(tpy)₂]²⁺ and **1a–c**, respectively. These should have been previously assigned to $^1[(d(\pi)_{\text{Ru}})^6] \rightarrow ^3[d(\pi)^5(\pi^*_{\text{tpy}})^1]$ MLCT, which become partially allowed due to the spin–orbital coupling, which has the effect of mixing the singlet and triplet excited-state manifolds.^{38,39}

As shown in Figure 5, computer deconvolution absorption bands at 546 nm ($\epsilon = 14\,000 \text{ M}^{-1} \text{ cm}^{-1}$) for **1a**, at 555 nm ($\epsilon = 20\,000 \text{ M}^{-1} \text{ cm}^{-1}$) for **1b**, and at 559 nm ($\epsilon = 14\,000 \text{ M}^{-1} \text{ cm}^{-1}$) for **1c** are apparent in the

(34) Bhadbhade, M. M.; Das, A.; Jeffery, J. C.; McCleverty, J. A.; Navas Badiola, J. A.; Ward, M. D. *J. Chem. Soc., Dalton Trans.* **1995**, 2769.

(35) Sohn, Y. S.; Hendrickson, D. N.; Gray, H. B. *J. Am. Chem. Soc.* **1971**, 93, 3603.

(36) Bazak, R. E. *Adv. Photochem.* **1971**, 8, 227.

(37) Braddock, J. N.; Meyer, T. J. *J. Am. Chem. Soc.* **1973**, 95, 3158.

(38) Kober, E. M.; Meyer, T. J. *Inorg. Chem.* **1982**, 21, 3967.

(39) Coe, B. J.; Thompson, D. W.; Culbertson, C. T.; Schoonover, J. R.; Meyer, T. J. *Inorg. Chem.* **1995**, 34, 3385.

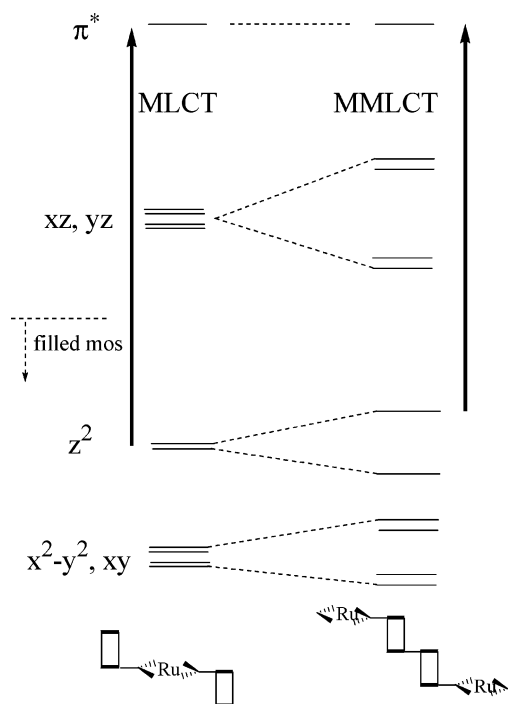


Figure 6. Schematic diagram of the orbital splittings and the proposed Fe–Fe interaction mode.

visible region. In the case of Ru^{2+} transition metal complexes containing ferrocenyl moieties, an intense broad structureless band in the 520 nm region has been observed.^{3,24,40} For the $[\text{Ru}(\text{fctpy})_2]^{2+}$ compound, a band at 526 nm ($\epsilon = 15\,000\ \text{M}^{-1}\ \text{cm}^{-1}$) is apparent.²⁴ This band is assigned to the $^1[(d(\pi)_{\text{Fe}})^6] \rightarrow ^1[(d(\pi)_{\text{Fe}})^5(\pi^*_{\text{tpy}}^{\text{Ru}})^1]$ transition.³ The intensity of this transition scales with the number of ferrocenyl substituents, and it disappears upon the oxidation of ferrocene. In our studies, this band is not present in the parent neutral compounds (**4**, tpy-(fc)_n-tpy), but coordination with Ru^{2+} metal centers results in a red-shifted and more intense transition in the visible region for **1b** and **1c** relative to the $[\text{Ru}(\text{fctpy})_2]^{2+}$ complex. The observed red-shifted absorption from 525 nm in monomeric complex $[\text{Ru}(\text{fctpy})_2]^{2+}$ to ~ 560 nm in **1b** and **1c** and a concomitant increase of the intensity of this band indicate that there is a qualitative electronic coupling within the ferrocenyl

(40) Benniston, A. C.; Goulet, V.; Harriman, A.; Lehn, J.-M.; Marczinke, B. *J. Phys. Chem.* **1994**, *98*, 7798.

array. This is consistent with the electrochemical behavior discussed above. As shown in Figure 6, the filled $3d_{x^2-y^2,xy,z^2}$ and empty $3d_{xz,yz}$ orbitals on each Fe^{2+} ion would overlap with each other, resulting from Fe–Fe interactions, leading to an absorption band in the red characteristic of the $^1[(d(\pi)_{\text{Fe}})^6] \rightarrow ^1[(d(\pi)_{\text{Fe}})^5(\pi^*_{\text{tpy}}^{\text{Ru}})^1]$ MMLCT transition.

Conclusion

We have prepared a series of polynuclear redox active supramolecules with the functionalized 1,1'-bis(terpyridyl)biferrocene and 1,1'-bis(terpyridyl)triferrocene ligands. Spectroscopic data show that the use of suitable metal ions such as Ru^{2+} will prove to be versatile in building molecular wires. The tpy-(fc)_n-tpy spacer plays a more sensitive role in gauging the interaction between the Ru^{2+} and Fe^{2+} centers. The positive potential shift of the $E_{1/2}$ values and the decreasing of $\Delta E_{1/2}$ value for the $\text{Fe}^{2+}/\text{Fe}^{3+}$ redox couples upon the coordination of the Ru^{2+} ion indicate that there is an interaction between Ru^{2+} and Fe^{2+} centers. Furthermore, the observed red-shifted absorption from 526 nm in the monomeric $[\text{Ru}(\text{fctpy})_2]^{2+}$ complex to ~ 560 nm in **1b** and **1c** reveals that there is a qualitative electronic coupling within the ferrocenyl array. The Fe–Fe interactions result in a red shift characteristic of the $^1[(d(\pi)_{\text{Fe}})^6] \rightarrow ^1[(d(\pi)_{\text{Fe}})^5(\pi^*_{\text{tpy}}^{\text{Ru}})^1]$ MMLCT transition. Compounds of tpy-(fc)_n-tpy potentially have the capability to coordinate transition metals, demonstrating the versatility in molecule assembly and generation of various composites. Expansion of this study to manipulate the energetics between the terminal metal center, such as Fe^{2+} ion, and the connecting spacer is underway and will be reported in due course.

Acknowledgments are made to the National Science Council (NSC92-2113-M-110-011), Taiwan, ROC, and Department of Chemistry and Center for Nanoscience and Nanotechnology at National Sun Yat-Sen University.

Supporting Information Available: Complete tables of positional parameters, bond distances and angles, and thermal parameters for **3**. This material is available free of charge via the Internet at <http://pubs.acs.org>.

OM0503040